Glassy and crystalline sodium ternary chalcogenide materials in the Na–As–Se system: Synthesis, properties and relation to crystallization

A. Sammoury, M. Kassem, Maria Bokova, Tayssir Hamieh, J. Toufaily, Eugène Bychkov

Open Ceramics 16 (2023) 100434

Contents lists available at ScienceDirect

Open Ceramics

journal homepage: www.sciencedirect.com/journal/open-ceramics

Glassy and crystalline sodium ternary chalcogenide materials in the Na–As–Se system: Synthesis, properties and relation to crystallization

A. Sammoury [a,b], M. Kassem [a,*], M. Bokova [a], Tayssir Hamieh [b,c], J. Toufaily [b], E. Bychkov [a]

[a] Université du Littoral Côte d'Opale (ULCO), LPCA, EA 4493, F-59140, Dunkerque, France
[b] MCEMA and LEADDER Laboratories, Faculty of Sciences and EDST, Lebanese University, Hariri Campus, Beirut, Lebanon
[c] Faculty of Science and Engineering, Maastricht University, P.O. Box 616, 6200 MD, Maastricht, the Netherlands

ARTICLE INFO

Handling Editor: Dr Catherine Elissalde

Keywords:
Sodium chalcogenide compounds
Glass/crystal preparation
XRD
SEM
Macroscopic properties
Electric conductivity
Thermal treatment

ABSTRACT

Sodium chalcogenide compounds, glassy and crystalline, are promising materials for a number of potential applications in non-linear optics (NLO), photovoltaic, and energy conversion and storage. This work deals with the study of the newly synthesized glasses in the Na_2Se–As_2Se_3 chalcogenide system as well as the corresponding ternary crystals, $NaAsSe_2$ and Na_3AsSe_3. We examine the glass-forming domain in the pseudo-binary system using melt-quenching and mechanical milling techniques. We also analyse the macroscopic and electrical properties of the glasses in comparison with their crystalline counterparts, and the annealed glasses yielding glassy/crystalline alloys.

1. Introduction

Glassy and crystalline sodium ternary chalcogenide materials appear to be promising for a large number of applications. They are receiving increased attention as infrared second-order nonlinear optical (NLO) materials, e.g. $NaGa_3Se_5$, $Na_2In_4SSe_6$, $NaIn_3Se$, $NaGaIn_2Se_5$ [1,2]. The 3D polyanionic network, build of 12 kinds of $GaSe_4$ tetrahedra in $NaGa_3Se_5$, represents a new NLO functional motif [1]. $NaInS_{2-x}Se_x$ compounds (x = 0.5, 1.0, 1.5) are potentially useful as optoelectronic materials under visible light exposure [3]. The sodium bismuth dichalcogenides NaBiS2 and NaBiSe2 show properties of interest for applications in energy conversion [4]. In addition, first-principles calculations show that the two compounds can be promising candidates of combining both functions of non-volatile memories and efficient manipulation of signals [5]. Ternary chalcogenide materials are also of interest for both photovoltaic and thermoelectric applications [6–9]. This includes compounds of the form $NaAX_2$ (A = As, Sb, and Te; X = S, Se, and Te) [10]. The direct band gaps found in $MAsQ_2$ (M = Li, Na; Q = S, Se) can be tuned by proper substitution of the alkali metals and chalcogens to lie in the spectral range that is optimal for photovoltaic applications [11].

Another important application for glassy and crystalline sodium materials is energy storage. Active development of solid-state batteries, especially those utilizing sodium electrolytes instead of lithium, is necessary to achieve high-capacity energy storage for both portable electronics and large stationary applications [12–17]. This is due to the cost-effectiveness and significantly higher abundance of sodium compared to lithium, making it a promising alternative. Research in this area has increased significantly as a result of the discovery of cubic Na_3PS_4, which, when crystallized from the glassy state, shows room-temperature ionic conductivity σ_{298} of 0.2 mS cm^{-1} [18]. The substitution of sulphur, in the Na_3PS_4 crystal, with selenium leads to $\sigma_{298} \approx 1.16$ mS cm^{-1} [19]. Other superionic sodium chalcogenides ($Na_{10}SnP_2S_{12}$, Na_3SbS_4, $Na_{11}Sn_2SbS_{12}$, $Na_{11}Sn_2SbSe_{12}$, $Na_{11}Sn_2PS_{12}$, etc.) were also reported [20–24]. Additionally, sodium-containing chalcogenide glasses have been documented in the literature, including Na_2Se–Ga_2Se_3-$GeSe_2$, Na_2Se–P_2Se_5, Na_3PS_4–NaI, Na_2S-GeS_2, Na_2S–As_2S_3, etc. [25–29].

In this study, the two different synthesis techniques, melt-quenching and mechanical milling, were used to explore the glass-forming region of the Na_2Se–As_2Se_3 system. Furthermore, the investigation encompassed an analysis of the macroscopic, thermal, morphological and electric properties to fully comprehend the impact of sodium selenide Na_2Se addition on the g-As_2Se_3 host network. Given that rapid ion-conducting glasses has been successfully obtained for silver-based selenide

* Corresponding author. Université du Littoral Côte d'Opale, LPCA, 189A avenue M. Schumann, 59140, Dunkerque, France.
E-mail address: Mohamad.Kassem@univ-littoral.fr (M. Kassem).

https://doi.org/10.1016/j.oceram.2023.100434
Received 18 June 2023; Received in revised form 13 August 2023; Accepted 15 August 2023
Available online 16 August 2023

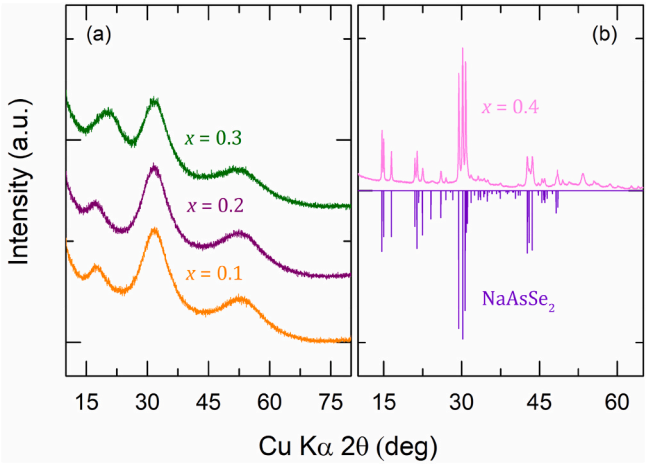

Fig. 1. (a) X-ray diffraction pattern for the x = 0.10, 0.20 and 0.30 glass compositions in the $(Na_2Se)_x(As_2Se_3)_{1-x}$ system. (b) Diffraction pattern for the x = 0.40 composition exhibit Bragg peaks corresponding to the orthorhombic $NaAsSe_2$, space group *Pbca* [34].

compounds such as $Ag_xAsSe_{1.5}$ [30] and Ag_2Se–As_2Se_3 [31], the host glass g-As_2Se_3 holds promise as a viable candidate for producing fast-ion conducting glasses that incorporate sodium. Our primary goal in conducting this research is to replicate the approach utilized for silver compounds to achieve sodium superionic glasses. We note that crystalline Na_2Se, insulator for transferring electrons, adopts a Fluorite structure and undergoes crystallization within the cubic Fm3m space group [32,33]. Additionally, we have synthesized and characterised the $NaAsSe_2$ crystal and, whenever feasible, we made comparisons between the properties of the glasses and the ternary Na–As–Se crystalline counterparts, i.e., $NaAsSe_2$ and Na_3AsSe_3.

2. Experimental section

2.1. Glass synthesis

Bulk $(Na_2Se)_x(As_2Se_3)_{1-x}$ alloys, $0.0 \leq x \leq 0.4$, were synthesized using the conventional melt quenching method. High-purity elements Na (Sigma-Aldrich, 99.9%), Se (Sigma-Aldrich, 99.999%) and previously synthesized glassy As_2Se_3 are mixed in appropriate proportions. The 1 g batches were placed in vitreous carbon crucibles in evacuated silica ampoules (8 mm ID/10 mm OD) that are then sealed under vacuum (10^{-6} mbar). The ampoules were heated in a furnace (heating rate 1 °C/min), kept at 750 °C for 24 h and finally cooled down and quenched in ice-cold water at 600−650 °C depending on x.

The planetary micro-mill Pulverisette 7 premium line (Fritsch GmbH, Germany) was used to prepare the mechanically-milled MM-$(Na_2Se)_{0.4}(As_2Se_3)_{0.6}$ sample. The previously prepared crystalline x = 0.40 composition (obtained by melt quenching) was milled under argon atmosphere in a 45 ml zirconia jar using ZrO_2 grinding balls (18 balls with 10 mm in diameter) at a maximum speed of 550 rounds per minute (rpm).

2.2. Crystal synthesis

The thermal synthesis procedure was used in the synthesis of crystals that exist in the Na–As–Se system, i.e., $NaAsSe_2$ and Na_3AsSe_3. For the $NaAsSe_2$ (25 at.% Na), the compounds Na, Se and As_2Se_3 were introduced to an evacuated silica tube in a ratio 2:1:1, heated to 750 °C and homogenized for 24h before slowly cooled down to room temperature during 8 h, Fig. S1 in supporting information. The same compounds were used in the synthesis of the Na_3AsSe_3 composition (42.87 at.% Na). The mixture, prepared using the ratio was 3:1.5:2, was heated slowly to 600 °C, homogenized at this temperature before being cooled down to 440 °C and annealed at this temperature for 3 days and then brought down to room temperature. The diffraction pattern acquired does not correspond to that of a pure Na_3AsSe_3 crystal. Therefore, throughout the article, we will base our discussion on existing literature data whenever this composition is involved.

2.3. XRD experiments

Amorphous and crystalline nature of the alloys was determined from X-ray diffraction experiments (XRD). A Bruker D8 Advance diffractometer, equipped with a copper anticathode emitting Kα radiation, a LinxEye detector, a goniometer θ/θ and a rotating sample holder, was used for this purpose. Measurements of scattering intensities were conducted by setting the 2θ angular range between 10° and 80° with a step-size of 0.02° and a count time of 2 s per step.

2.4. Density measurement

The density d values were obtained, using a Sartorius YDK 01-OD density kit at room temperature, for 0.5−1.5 g samples. To this end, a hydrostatic method using toluene as immersion fluid and germanium (5.323 g cm^{-3}) as reference was employed.

2.5. Scanning electron microscopy (SEM) experiments

SEM analysis was performed using a JEOL JSM-7100F thermal field emission scanning electron microscope equipped with EDX Bruker QUANTAX 800 spectrometers.

2.6. DSC measurements

Using the TA Instruments Q200 thermal analyser, Differential scanning calorimetry (DSC) experiments were conducted to determine the characteristic temperatures of glass, i.e., the glass transition Tg, the crystallization Tx and the melting Tm temperatures. The hermitically sealed aluminium pan containing 5−10 mg sample was heated at a rate of 10 °C per minute, under dry nitrogen atmosphere, in the range 20–450 °C. To determine the average glass transition temperature, three measurements were typically conducted for each composition.

2.7. Electrical conductivity measurements

The Hewlett Packard 4339B high resistance meter was employed to evaluate the direct current dc electrical conductivity of the obtained glassy and crystalline samples in the Na–As–Se system. The measurement were performed, using an applied voltage of 100 V, from room temperature to a nearly glass transition (T_g − 20 °C). Silicon carbide powder (9.3 μ grain size) was used to produce rectangular plates (4–6 mm^2 area and 0.8–1.4 mm thickness) from the as-prepared samples. For the MM and crystalline samples, a Jasco 25 tons motorized press was used to prepare disc pellets with a diameter of 13 mm and a thickness of 0.8–1.1 mm. For both sample forms, gold was sputtered on the two opposite sides as electrodes. The electrical conductivity was calculated from the sample resistance R and the geometrical factor L/A (where L represents the thickness of the sample and A denotes the area of gold contact).

3. Results and discussion section

3.1. Na_2Se–As_2Se_3 system: glass-forming domain

XRD patterns of the bulk $(Na_2Se)_x(As_2Se_3)_{1-x}$ alloys, $0.0 \leq x \leq 0.4$, prepared by melt quenching synthesis method, are presented in Fig. 1. The vitreous domain in this system is rather limited with $x_{max} = 0.3$. The broad diffraction bands, Fig. 1(a), are an indicative of the glassy state of

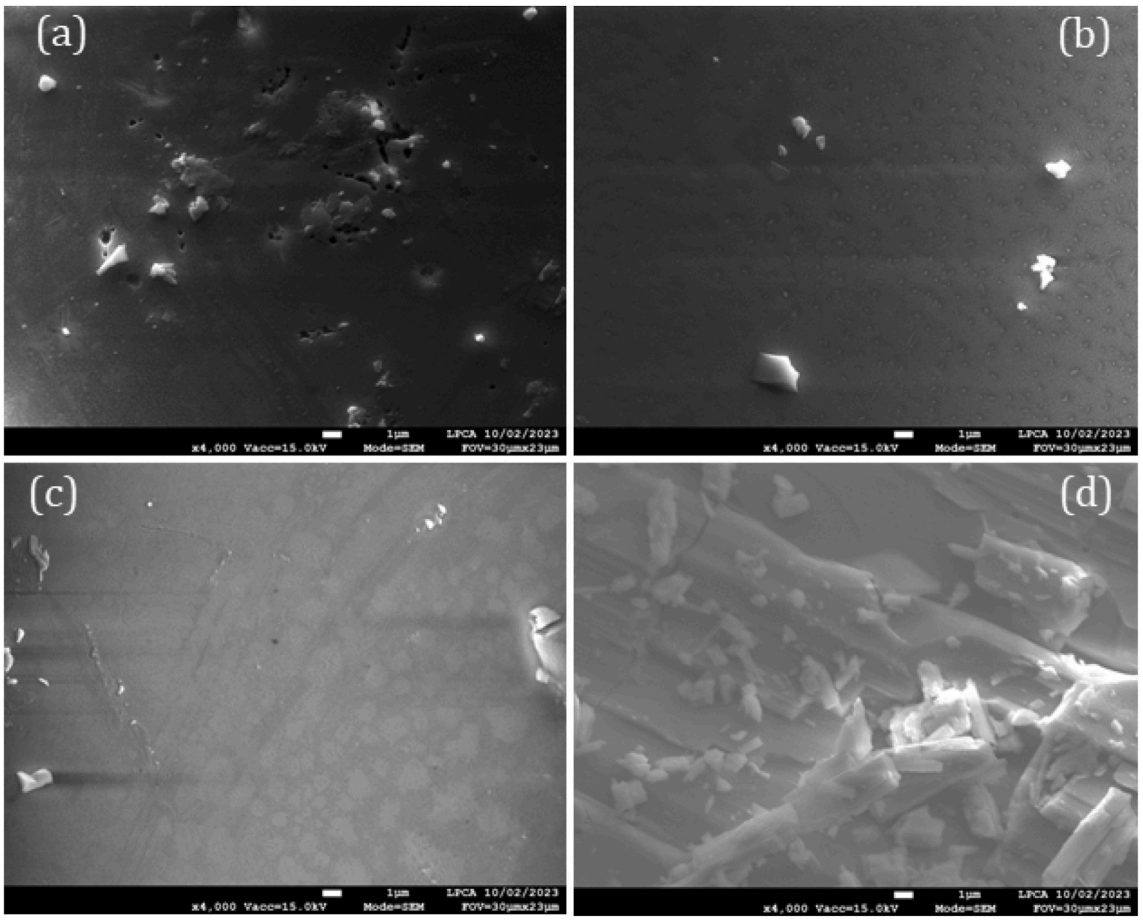

Fig. 2. (a) SEM images of the three glass compositions in the $(Na_2Se)_x(As_2Se_3)_{1-x}$ system, i.e., (a) $x = 0.10$, (b) $x = 0.20$, (c) $x = 0.30$ and (d) the crystalline $x = 0.40$ composition.

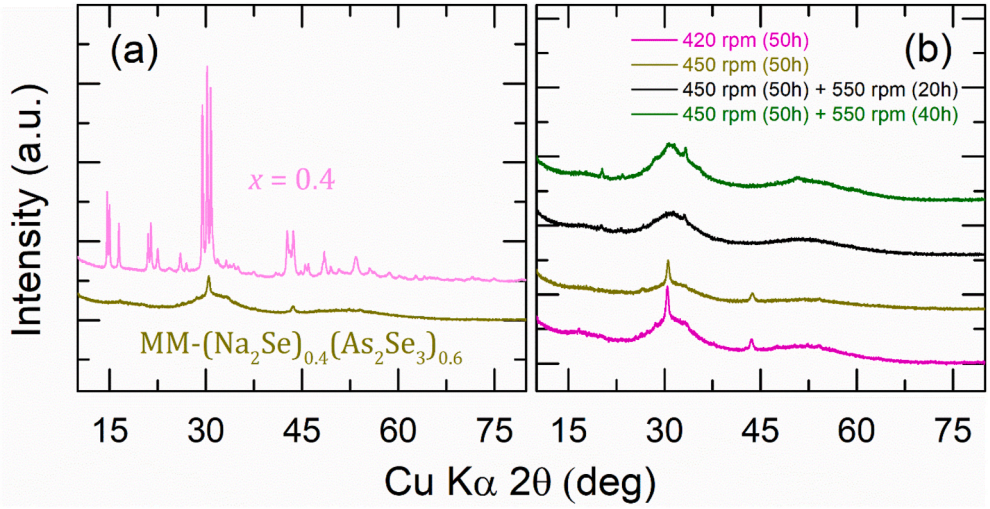

Fig. 3. (a) X-ray diffraction patterns for the $x = 0.40$ composition obtained by melt quenching in silica tubes and mechanical milling at 450 rmp for 50 h. (b) XRD spectra of the MM-$(Na_2Se)_{0.4}(As_2Se_3)_{0.6}$ sample at different mechanical-milling conditions.

the compositions $x = 0.1$, 0.2 and 0.3. For the synthesized compositions at $x > 0.3$, Bragg peaks appear. Fig. 1(b) shows that the XRD pattern of the as-prepared sample $x = 0.4$ is characteristic of the orthorhombic phase $NaAsSe_2$, space group *Pbca* [34].

To investigate the morphology of the obtained as-prepared melt-quenched samples, we conducted a scanning electron microscopy (SEM) of the four samples $x = 0.10$, 0.20, 0.30 and 0.40 in the $(Na_2Se)_x(As_2Se_3)_{1-x}$ alloys, Fig. 2. The morphology is quite different from one composition to another. Fig. 2(a) shows that the surface is mostly homogeneous for the $x = 0.10$ composition despite some evident roughness and porosity. The $x = 0.20$ composition exhibits distinctive nano-structure features (Fig. 2(b)), comprising nano-rods approximately 500

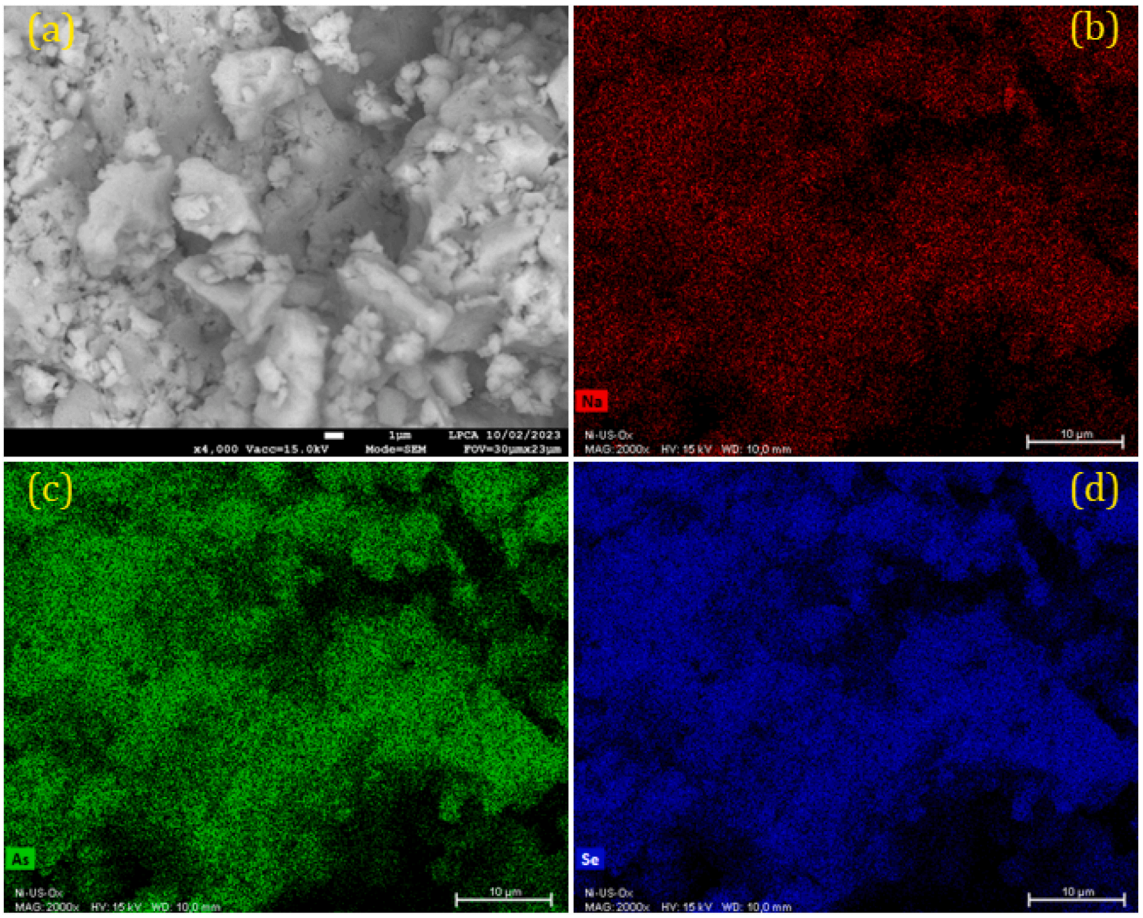

Fig. 4. (a) SEM image of the MM-$(Na_2Se)_{0.4}(As_2Se_3)_{0.6}$ sample after the milling duration of 90 h and (b–d) energy-dispersive X-ray spectroscopy (EDX) element mapping of Na(red), As (green), and Se (blue), respectively. (For interpretation of the references to colour in this figure legend, the reader is referred to the Web version of this article.)

Table 1
Density (d), mean atomic volume (V_a), and glass packing density (ρ) of the $(Na_2Se)_x(As_2Se_3)_{1-x}$ samples with $0.0 \leq x \leq 0.4$.

Na_2Se content (x)	d (g cm^{-3})	V_a (cm^3 mol^{-1})	ρ
0.00	4.61 (3)	16.77 (11)	0.712 (4)
0.05	4.59 (2)	16.62 (7)	0.711 (3)
0.10	4.56 (1)	16.46 (4)	0.711 (1)
0.15	4.51 (1)	16.37 (5)	0.707 (2)
0.20	4.46 (2)	16.31 (7)	0.702 (3)
0.25	4.39 (1)	16.23 (3)	0.697 (2)
0.30	4.32 (1)	16.21 (4)	0.689 (2)
0.35[a]	4.25 (6)	16.12 (23)	0.683 (9)
0.40[a]	4.18 (4)	16.04 (15)	0.677 (6)
Na–As–Se crystals			
$NaAsSe_2$ (this work)	3.92 (9)	16.31 (37)	0.645 (14)
$NaAsSe_2$ [36]	4.04	15.83	0.664
Na_3AsSe_3 [37]	3.61	15.07	0.631

Uncertainties in the last digit(s) of the parameter are given in parentheses.
[a] *Glassy/crystalline samples*.

nm in length, alongside a considerably larger quantity of nanospheres measuring just a few nanometers in size. This characterization is further evident in Fig. S2, which displays SEM images of this composition at different magnifications, i.e., × 12000 and × 20000. The surface morphology of the $x = 0.30$ sample displays easily discernible droplet-like macrostructures of various sizes, from 1 µm or less up to 4–6 µm, Fig. 2(c) and Fig. S3 (supporting information). This indicates that the compositions at $x \geq 0.2$ are phase-separated. The morphology of the crystalline $x = 0.40$ composition is largely different; structures of various shapes and sizes are observed, Fig. 2(d).

Using the mechanical milling (MM) technique, we have tried to expand the vitreous domain further, and the results are presented in Fig. 3. XRD patterns of the MM-$(Na_2Se)_{0.4}(As_2Se_3)_{0.6}$ sample are significantly dependent on the utilized mechanical-milling conditions. The milling of the as-prepared $x = 0.4$ sample, at a speed of 420 and 450 round per minute (rpm) for a duration of 50 h (50 h), lead to the disappearance of the majority of the peaks of the orthorhombic $NaAsSe_2$ phase. Only two narrow intense peaks persist and are reminiscent of the orthorhombic phase, Fig. 3(b) (magenta and dark yellow curves). No further changes were seen when the milling duration was increased beyond 50 h at these two conditions. The two peaks disappear completely when an extra milling condition (550 rpm) is added to the previous one at 450 rpm for 50 h. Two different duration periods for 20 and 40 h were employed (black and green curves), Fig. 3(b). The XRD patterns contained a halo indicating the formation of the amorphous phase, but two newly emerged undefined peaks with low intensity appear. The vitreous phase represents the major part of the MM-$(Na_2Se)_{0.4}(As_2Se_3)_{0.6}$ sample and hence is classified as glass ceramic.

Fig. 4(a) displays a SEM micrograph for the powdered glass-ceramic MM-$(Na_2Se)_{0.4}(As_2Se_3)_{0.6}$ composition. Morphologies of different forms are present. This includes micro− and nano−sized particles as well as nanometer diameter fibers that are several micrometers long. Also, the morphology and element distribution of the MM-$(Na_2Se)_{0.4}(As_2Se_3)_{0.6}$ sample was analysed using EDX. It is found that the sodium, arsenic and selenium constituent elements are uniformly scattered all over the MM-glass ceramic, Fig. 4(b)–(d).

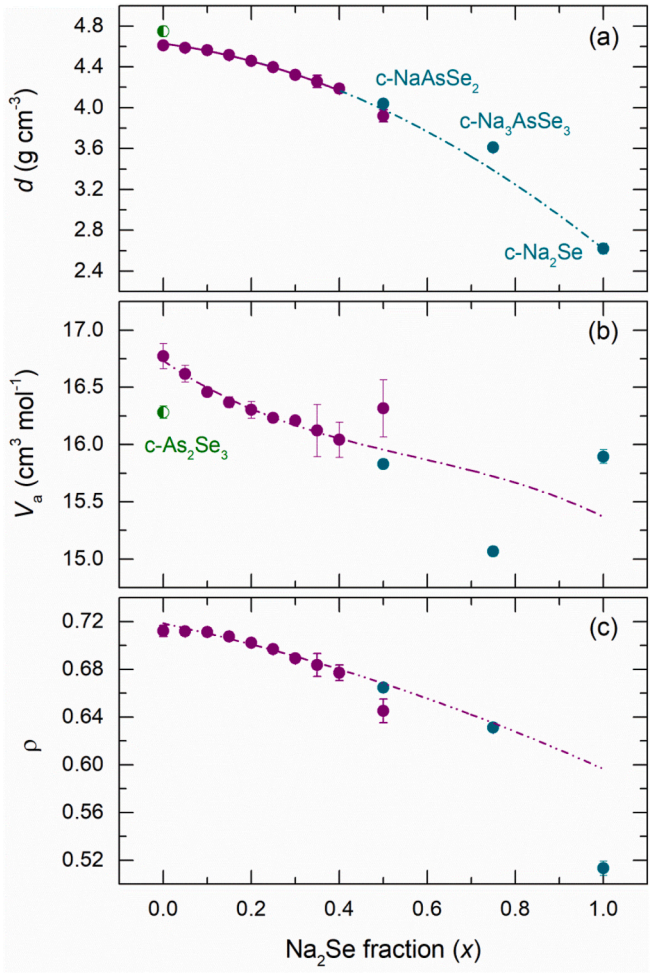

Fig. 5. (a) Density, (b) mean atomic volume and (c) glass/crystal packing density of the $(Na_2Se)_x(As_2Se_3)_{1-x}$ alloys plotted as a function of the sodium selenide content. The crystalline data of c-As_2Se_3 [35], c-$NaAsSe_2$ [36], c-Na_3AsSe_3 [37] and c-Na_2Se [38] are also plotted.

Table 2
The characteristic temperatures and glass-forming criteria in the $(Na_2Se)_x(As_2Se_3)_{1-x}$ samples: glass transition T_g, crystallization temperatures T_x, melting temperatures T_m, the parameter $\Delta T = T_{x1} - T_g$, and Hruby criterion $H_r = (T_{x1} - T_g)/(T_{m1} - T_{x1})$.

Na_2Se content (x)	T_g (°C) (±3)	T_x (°C) (±3)			T_m (°C) (±3)		ΔT (°C) (±3)	H_r
		T_{x1}	T_{x2}	T_{x3}	T_{m1}	T_{m1}		
0.00	178	357	–	–	382	–	179	7.16
0.05	161	310	–	–	352	375	149	3.54
0.10	152	275	283	–	357	365	123	1.50
0.15	150	250	277	–	354	–	100	0.96
0.20	149	245	275	–	357	–	96	0.85
0.25	148	211	266	–	358	379	63	0.42
0.30	147	185	227	264	357	395	38	0.22
0.35[a]	146	176	224	264	357	415	30	0.16
0.40[a]	–	172	270	288	352	428	–	–

Uncertainties in the last digit(s) of the parameter are given in parentheses.
[a] *Glassy/crystalline samples.*

3.2. Na_2Se–As_2Se_3 system: density, mean atomic volume and packing density

The measured density (d) and the calculated mean atomic volume (V_a) and the packing density (ρ) values of the glassy, glassy-crystalline and crystal samples obtained in the Na_2Se–As_2Se_3 system are listed in Table 1 and plotted in Fig. 5. The V_a values were calculated using equation (1) where c_i is the atomic fraction of the element i, M_i the

Table 3
Conductivity parameters of glasses and crystals in the Na_2Se–As_2Se_3 system: the room-temperature conductivity σ_{298}, the activation energy E_σ, and the pre-exponential factor σ_0.

Composition			σ_{298} (S cm^{-1})	E_σ (eV)	σ_0 (S cm^{-1} K)
$(Na_2Se)_x(As_2Se_3)_{1-x}$ glasses and glassy/crystalline alloys					
x	[Na] *(at. %)*	r_{Na-Na} (Å)			
0.00	0.00	–	1.58×10^{-13}	1.038 (58)	2.8×10^5
0.05	2.04	13.72	9.91×10^{-13}	0.967 (7)	6.3×10^6
0.10	4.16	10.78	3.62×10^{-12}	0.936 (5)	7.1×10^6
0.15	6.38	9.33	8.31×10^{-12}	0.918 (6)	7.9×10^6
0.20	8.69	8.41	1.14×10^{-11}	0.910 (5)	8.1×10^6
0.25	11.11	7.74	1.27×10^{-11}	0.903 (5)	6.8×10^6
0.30	13.63	7.22	1.25×10^{-11}	0.883 (4)	3.2×10^6
0.35[a]	16.27	6.79	6.64×10^{-12}	0.846 (13)	3.9×10^5
0.40[a]	19.04	6.44	9.14×10^{-12}	0.842 (8)	4.7×10^5
MM-sample	19.04	6.44	4.08×10^{-8}	0.442 (18)	3.6×10^2
Na–As–Se crystals					
$NaAsSe_2$	25	5.91	4.31×10^{-15}	1.11 (1)	2.5×10^4
$NaAsSe_2$ [50]	25	5.85	7.22×10^{-15}	1.30	–
Na_3AsSe_3 [50]	42.87	4.81	9.15×10^{-15}	1.10	–

Uncertainties in the last digit(s) of the parameter are given in parentheses.
[a] *Glassy/crystalline samples.*

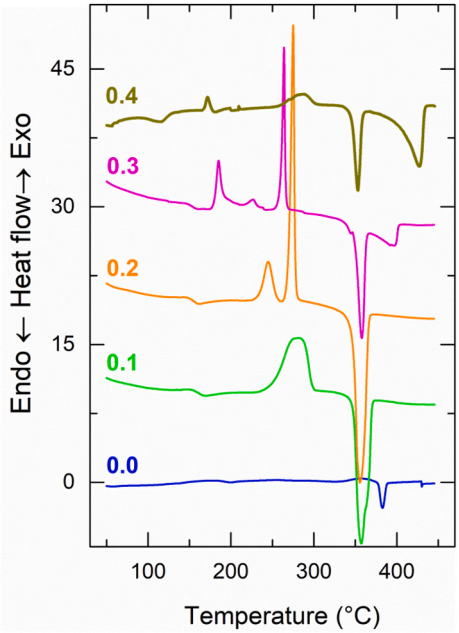

Fig. 6. DSC curves of the $(Na_2Se)_x(As_2Se_3)_{1-x}$ glasses, $0.0 \leq x \leq 0.3$ and MM-$(Na_2Se)_{0.4}(As_2Se_3)_{0.6}$ sample.

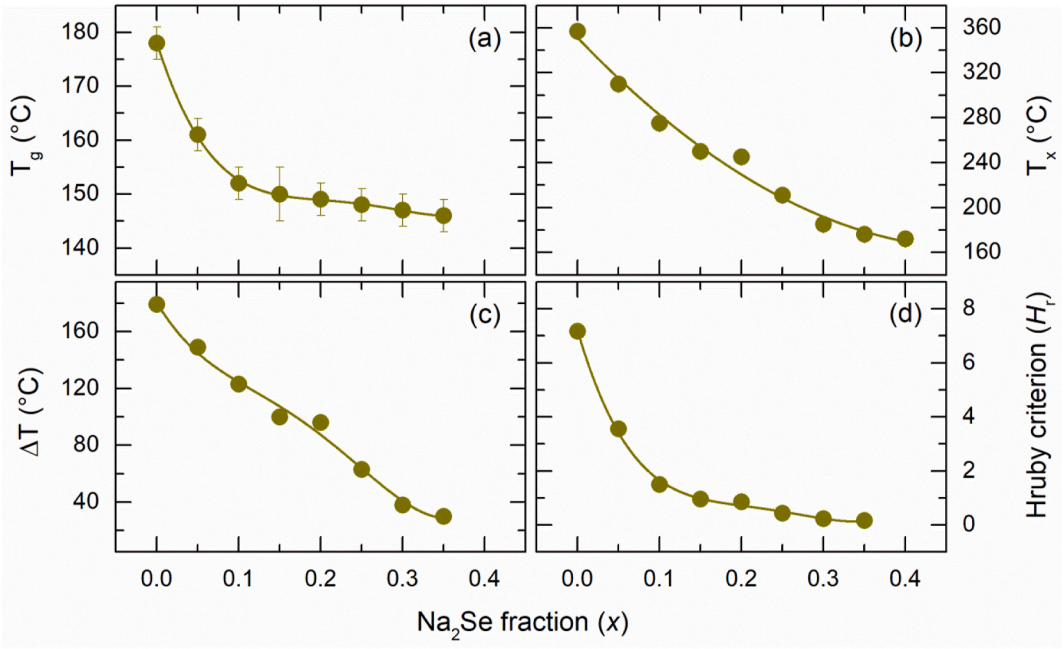

Fig. 7. (a) Glass transition *Tg*, (b) first crystallization peak *Tx*1, (c) empirical parameter ΔT and (d) Hruby criterion H_r of the $(Na_2Se)_x(As_2Se_3)_{1-x}$ samples, $0.0 \leq x \leq 0.4$. The lines are drawn as guide for the eyes.

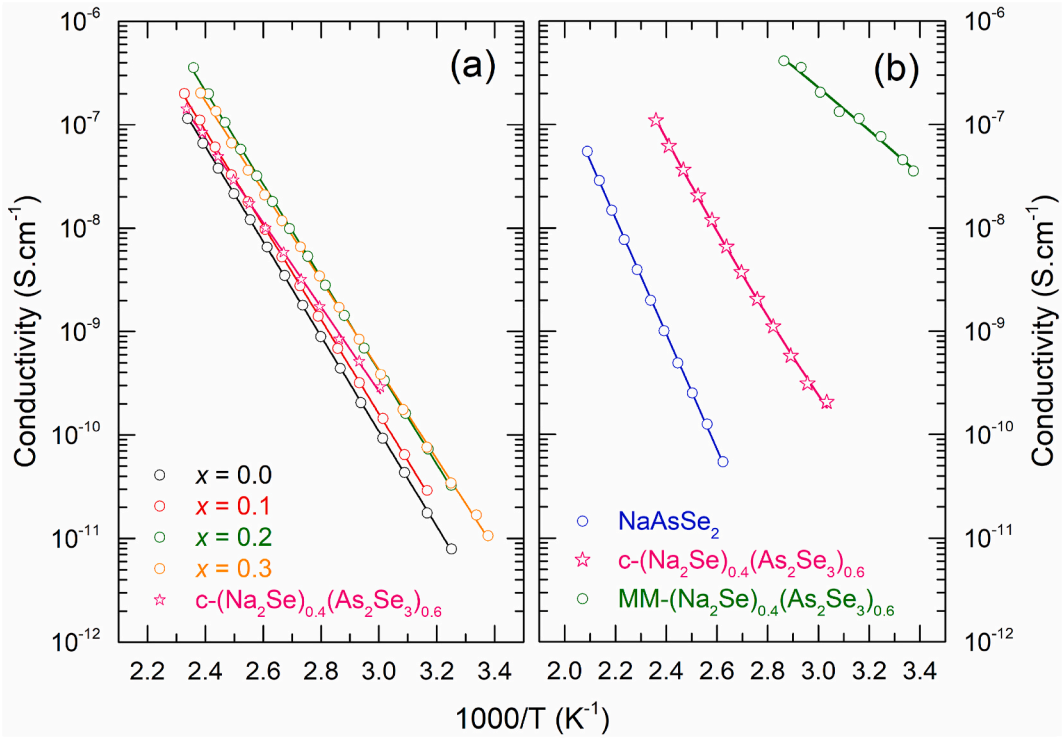

Fig. 8. (a) Direct current conductivity (σ_{dc}) plotted as a function of 1000/T for the $(Na_2Se)_x(As_2Se_3)_{1-x}$ samples obtained by melt-quenching, $0.0 \leq x \leq 0.4$. (b) σ_{dc} for the crystalline compound $NaAsSe_2$, the crystalline $x = 0.4$ composition, i.e., c-$(Na_2Se)_{0.4}(As_2Se_3)_{0.6}$ and the MM-$(Na_2Se)_{0.4}(As_2Se_3)_{0.6}$. The solid lines represent the least-square fit of the data of equation (4).

atomic mass, N_A the Avogadro constant and d is the density. Equation (2) was utilized to calculate the values of ρ, defined as the ratio between V_a^0 and V_a; V_a^0 is the average atomic volume of the sample constituents that is calculated using composition stoichiometry and the Shannon covalent radii r_i (equation (3)).

$$V_a = \frac{\sum_i C_i M_i}{dN_A} \quad (1)$$

$$\rho = \frac{V_a^0}{V_a} \quad (2)$$

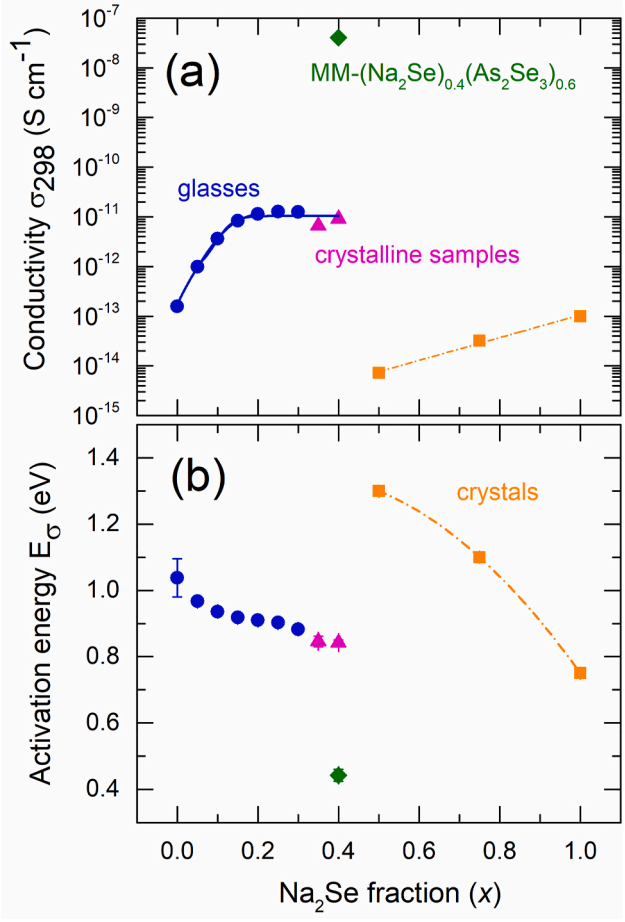

Fig. 9. (a) Room-temperature conductivity σ_{298}, (b) Activation energy E_σ plotted as a function of sodium selenide fraction for glass samples (dark blue circles), crystalline samples (magenta triangles), mechanical-milling MM-$(Na_2Se)_{0.4}(As_2Se_3)_{0.6}$ (dark green diamond) and the crystals $NaAsSe_2$, Na_3AsSe_3, and Na_2Se (orange squares). The Na_2Se data were taken from Ref. [32]. (For interpretation of the references to colour in this figure legend, the reader is referred to the Web version of this article.)

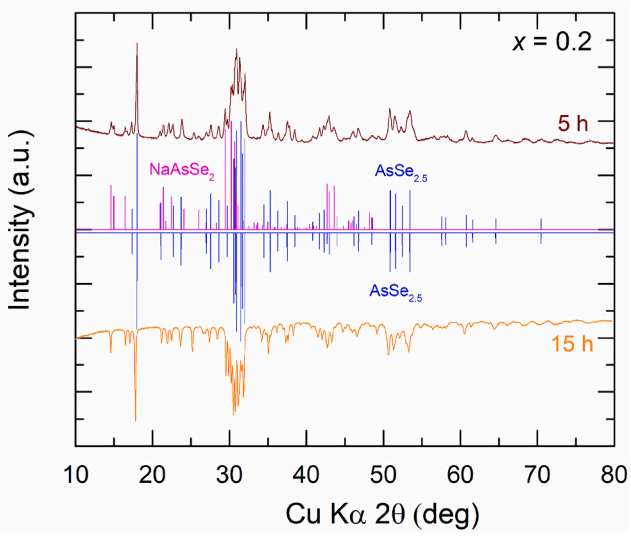

Fig. 10. X-ray diffraction patterns for the $x = 0.20$ glassy composition annealed at 275 °C for 5 h and 15 h.

$$V_a^0 = \sum_i c_i \frac{4\pi}{3} r_i^3 \quad (3)$$

The density variations as a function of the sodium selenide molar content x are shown in.

Fig. 5(a). The density decreases steadily with increasing x. In the vitreous domain at $x \leq 0.3$, the glass densities are in the range 4.61−4.32 g cm^{-3}. This is anticipated considering that the density of the crystalline $c-Na_2Se$ ($d_{Na2Se} = 2.62$ g cm^{-3} [35]) is lower than that of the glassy $g-As_2Se_3$ matrix ($d_{g\text{-}As2Se3} = 4.61$ g cm^{-3}) or crystalline $c-As_2Se_3$ ($d_{c\text{-}As2Se3} = 4.75$(g cm^{-3} [35]). We note that even the crystallization of the compositions $x = 0.35$ and $x = 0.4$ does not alter this tendency. Also, this tendency persists for the two known Na–As–Se crystal compounds, i.e., $NaAsSe_2$ ($d_{NaAsSe2} = 3.92$ (this work) and $d_{NaAsSe2} = 4.04$ [36]) and Na_3AsSe_3 ($d_{Na3AsSe3} = 3.61$ [37]), Table 1. The extrapolation to $x = 1$ gives for hypothetical glassy $g-Na_2Se$ a density value similar to that of $c-Na_2Se$, Fig. 5(a).

The composition dependence, as a function of sodium selenide, of both V_a and ρ, is shown in Fig. 5(b) and (c), respectively. The V_a curve decreases gradually from 16.77 ± 0.11 cm^3 mol^{-1} ($x = 0.0$) to 16.04 ± 0.15 cm^3 mol^{-1} ($x = 0.3$) and its extrapolation to a hypothetical $g-Na_2Se$ at $x = 1$ hints for a denser packing of the later compared to cubic $c-Na_2Se$. The glass packing density is constant up to $x = 0.1$ and decreases gradually thereafter (at $x > 0.1$) suggesting a less compact g-As_2Se_3 network structure with increasing x. However, despite such decrease, the glass compounds still present higher packing density values compared to the crystal compounds, Fig. 5(c). This might be related to lower sodium coordination number N_{Na-Se} and shorter r_{Na-Se} interatomic distances in glasses compared to $NaAsSe_2$ ($N_{Na-Se} = 6$, $r_{Na-Se} = 2.98-3.18$ Å) [36], Na_3AsSe_3 ($N_{Na-Se} = 6$, $r_{Na-Se} = 2.99-3.33$ Å) [37] and cubic $c-Na_2Se$ ($N_{Na-Se} = 4$, $r_{Na-Se} = 2.93$ Å) [38]. Also, the selenium coordination number varies for the crystals ($N_{Se-Na} = 8$ for Na_2Se, $N_{Se-X\ (X=Na+As)} = 7$ for Na_3AsSe_3 ($SeNa_6As$ pentagonal bi-pyramids), and $N_{Se-X\ (X=Na+As)} = 4$ and 5 for $NaAsSe_2$ ($SeNa_2As_2$ tetrahedra and Se Na_4As pyramids)) [36–38]. High-energy X-ray diffraction and neutron scattering experiments are planned to reveal the structure of glassy compositions.

3.3. Na_2Se–As_2Se_3 system: characteristic temperatures

The glass transition T_g, crystallization T_{x1}, T_{x2} and T_{x3} and melting T_{m1} and T_{m2} temperatures for the Na_2Se–As_2Se_3 system are summarized in Table 2. The ΔT parameter and the Hruby criterion H_r were used to evaluate the stability of the glasses system against crystallization. In this regard, $\Delta T = T_{x1} - T_g$ and $H_r = (T_{x1} - T_g)/(T_{m1} - T_{x1})$ where T_{x1} and T_{m1} corresponds to the first crystallization and melting peaks, respectively. The calculated values are also reported in Table 2.

Fig. 6 shows a typical DSC curves of the $(Na_2Se)_x(As_2Se_3)_{1-x}$ compositions, $x = 0.0$, 0.1, 0.2, 0.3 and 0.4. All the glassy compositions, i.e., $0.0 \leq x \leq 0.3$, present a single glass transition temperature. The expected second T_g, corresponding to the phase-separated sodium-rich glasses at $x \geq 0.2$, was absent even if the phase-separation was clearly evident from SEM. The exothermic crystallization and endothermic melting features can also be seen for all the DSC curves. Fig. 7(a) traces the glass transition evolution as a function of the sodium selenide content x. The decrease in T_g values is evident, but the rate of decrease varies. For $x \leq 0.1$ glasses, T_g experiences a significant drop of approximately 26 °C, going from 178 °C ($x = 0.0$) to 152 °C ($x = 0.1$). On the other hand, at $x > 0.1$, T_g is quasi-invariant and the change is roughly 4 °C. The reduction of T_g values in glasses is often linked to the progressive depolymerisation of the matrix network that involves the formation of non-bridging Se atoms. Similar outcomes have been observed in other systems when metal (Ag, Na) halides or selenides were incorporated, e.g. $(AgI)_x(As_2Se_3)_{1-x}$ [39], $(Ag_2Se)_x(Ga_2Se_3)_{0.1}(GeSe_2)_{1-x}$ [40] and $(Na_2Se)_x(Ga_2Se_3)_{1-x}(GeSe_2)_{0.75}$ [41].

As the Na_2Se content increases, the weak crystallization peak T_{x1} (x

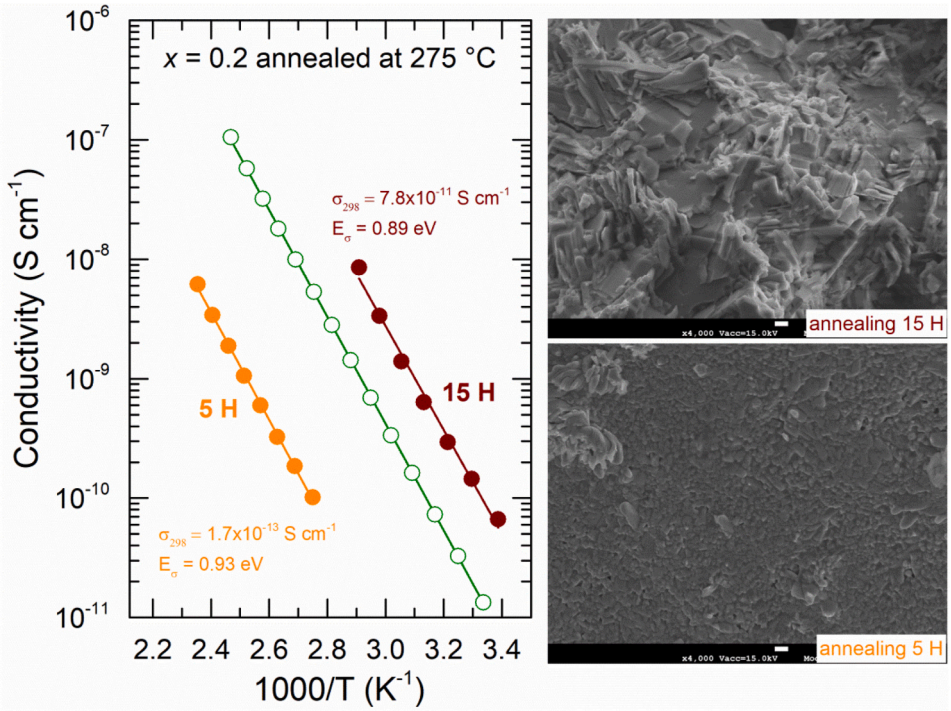

Fig. 11. Conductivity results of the $x = 0.2$ sample before (green colour) and after annealing at a temperature of 275 °C for two different durations: 5 h (orange colour) and 15 h (wine colour) and scanning electron microscope (SEM) micrographs for the annealed composition. (For interpretation of the references to colour in this figure legend, the reader is referred to the Web version of this article.)

= 0.0) becomes more pronounced and shifts to a lower temperature, Fig. 7(b). Two distinct crystallization peaks (T_{x1} and T_{x2}) are observed for the $x = 0.1$ composition and they become increasingly separated with increasing x. Furthermore, a third crystallization peak (T_{x3}) emerges at $x = 0.3$. Consequently, the introduction of sodium selenide reduces the resistance of the g-As_2Se_3 host matrix toward crystallization. The decreasing glass-forming ability is confirmed by the decrease in the values of criterions ΔT and H_r. The plots depicting the curves for ΔT and H_r are found in Fig. 7(c) and (d), respectively.

3.4. Na_2Se–As_2Se_3 system: electrical conductivity of glasses and crystals

Fig. 8 portrays the correlation between the temperature and the total direct current conductivity (σ_{dc}) of Na_2Se–As_2Se_3 glassy and crystalline samples for different Na_2Se fractions (x). Fig. 8(a) shows the results related to the melt-quenched glasses of $(Na_2Se)_x(As_2Se_3)_{1-x}$, ranging from $x = 0.0$ to $x = 0.3$, as well as the crystalline composition with $x = 0.4$.

In Fig. 8(b), the results for the crystalline orthorhombic compound $NaAsSe_2$, the mechanically milled glass-ceramic MM-$(Na_2Se)_{0.4}(As_2Se_3)_{0.6}$ sample, and the c-$(Na_2Se)_{0.4}(As_2Se_3)_{0.6}$ are displayed. It was observed that hysteresis, which can occur in some cases when examining the total electrical conductivity during heating and cooling cycles, was absent. The conductivity of different samples adheres to the Arrhenius law, as shown in equation (4).

$$\sigma = \frac{\sigma_0}{T} \exp\left(-\frac{E_a}{kT}\right) \quad (4)$$

where σ_0 is the conductivity pre-exponential factor, E_a the activation energy, k the Boltzmann constant and T the temperature. The room temperature conductivity σ_{298}, σ_0 and E_a were calculated from a least-square fit of the data to Eq. (4). The results are summarized in Table 3 and shown in Fig. 9.

The composition dependence of the conductivity parameters for Na_2Se–As_2Se_3 glasses and crystalline compounds are shown in Fig. 9. The room-temperature conductivity for the melt-quenched $(Na_2Se)_x(As_2Se_3)_{1-x}$ samples, $0.0 \leq x \leq 0.4$, increases by about 2 order of magnitude from 1.5×10^{-13} S cm^{-1} ($x = 0.0$) to 1.2×10^{-11} S cm^{-1} ($x = 0.3$), Fig. 9(a). The $(Na_2Se)_{0.25}(As_2Se_3)_{0.75}$ glass sample has the maximum room-temperature conductivity, 1.27×10^{-11} S cm^{-1}.

However, we note that the conductivity trend is not monotonic. Two different domains are clearly observed. In the first domain, $0.0 \leq x \leq 0.2$ (≤8.6 at.% Na), the conductivity increase is dependent on the Na_2Se content. This is no longer valid for the second domain, $0.2 \leq x \leq 0.4$ (8.6 ≤ [Na] ≤ 19.0 at.%). An apparent saturation of conductivity at high sodium content appears and the room-temperature conductivity is quasi-invariant even for the crystallized sample, i.e. for $x = 0.35$ and 0.4. Moreover, the activation energy show an overall decrease from 1.038 eV ($x = 0.0$) to 0.842 eV ($x = 0.4$), Fig. 9(b). Surprisingly, the glass-ceramic MM-$(Na_2Se)_{0.4}(As_2Se_3)_{0.6}$ sample shows much higher conductivity value, $\sigma_{298} = 4.08 \times 10^{-8}$ S cm^{-1}. Compared to the crystalline $x = 0.4$ composition, the conductivity increases by an astonishing four order of magnitude, Fig. 9(a), and this increase is accompanied by the lowest activation energy recorded for this system, $E_a = 0.44$ eV, Fig. 9(b). In comparison to the homogenous glasses in the Na_2Se–P_2Se_5 [42] (refer to Fig. S4), similar conductivity values are evident for $x \leq 0.1$. However, a departure from this trend becomes apparent when the sodium selenide content reaches $x \geq 0.2$, rendering the glasses in the Na_2Se–As_2Se_3 system electrically inert. This prompts the hypothesis that this inactivity might be connected to the inhomogeneity of bulk glasses at $x \geq 0.2$ as revealed from SEM. The nature of phase-separation in glasses, its existence or absence is of importance for conductivity parameters. Let's take, as an example, the silver thioarsenate glasses, $(Ag_2S)_x(As_2S_3)_{1-x}$, where $0.0 \leq x \leq 0.65$; the glasses are phase separated for the compositions $0.1 \leq x \leq 0.4$ (i.e. for Ag content comprised between ~4 and ~20 at.%) [43]. An abrupt increase in conductivity (σ) spanning 4 to 5 orders of magnitude is observed at ~7 at.% Ag [44]. This phenomenon occurs when silver-rich phase, initially embedded within the silver-poor phase, transitions into the dominant phase for silver concentrations exceeding 7 at.% and assumes the role of governing silver diffusion [45].

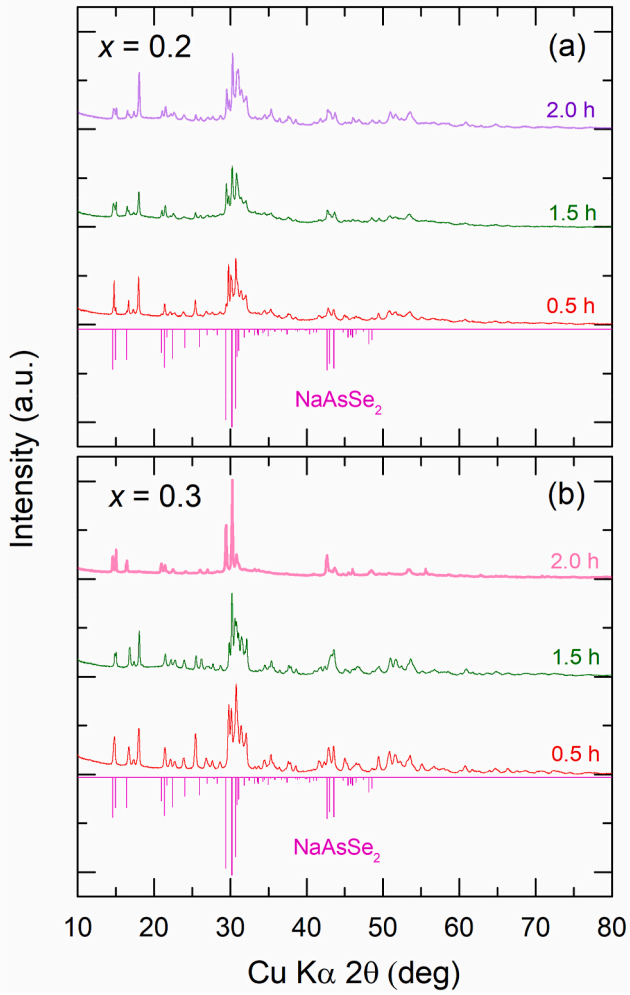

Fig. 12. X-ray diffraction patterns for the annealed (a) $x = 0.20$ and (b) $x = 0.30$ compositions; The annealing durations were 30 min, 1.5 h and 2 h at 275 °C.

Indeed, the structural motifs in homogeneous $(Ag_2S)_x(As_2S_3)_{1-x}$ glasses, where $x \geq 0.4$, are related to Ag_2S–As_2S_3 crystalline counterparts in $AgAsS_2$ ($x = 0.5$) and Ag_3AsS_3 ($x = 0.75$). A significant difference between the two families, i.e., homogeneous and phase-separated, resides in the absence of silver-poor crystalline compounds in Ag_2S–As_2S_3 system. Consequently, we can formulate a hypothesis that the lack of Ag-poor crystals (due to their thermodynamic instability), within a specific system, accounts for an extensive composition range of phase-separated glasses consisting of silver-poor and silver-rich glassy phases. Likewise, it can be postulated that the absence of sodium-poor crystalline compounds in Na_2Se–As_2Se_3 system contributes to the phase separation observed within the composition range of $0.1 \leq x \leq 0.3$. Furthermore, the absence of electrical activity might be linked to the prevalence of sodium-poor phases within the structural framework of the glass. The substantial increase in conductivity by four orders of magnitude observed in the MM-$(Na_2Se)_{0.4}(As_2Se_3)_{0.6}$ sample is indicative of a shift in change in the structural motifs governing the sodium diffusion. Notably, the conductivity value of this glass-ceramic matches that of Na_2Se–P_2Se_5, i.e., the $x = 0.4$ homogenous composition with same sodium selenide content (as shown in Fig. S4). This observation potentially implies that the mechanically-milled sample is either homogenous in nature or influenced to a certain extent by a sodium-rich phase. The pre-exponential value obtained for the mechanically-milled sample indicates the presence of a distinct sodium diffusion mechanism, as depicted in Fig. S5. Comparatively, the pre-exponential factor σ_0 for the glass-ceramic MM-$(Na_2Se)_{0.4}(As_2Se_3)_{0.6}$ sample is approximately 3.5 orders of magnitude lower than that observed in the melt-quenched Na_2Se–As_2Se_3 samples. For the latter, the σ_0 values remain notably invariant, falling within the range of $\sim 10^5 \leq \sigma_0(x) \leq \sim 10^6$ S cm^{-1} K. This constant pre-exponential factor is frequently noted in ion-conducting sulfide glasses, even across a wide composition range [46–48] and has been attributed to the contrasting trends in composition, i.e., the effective jump distance $l(x)$, decreasing with x, the cation content $C(x)$, increasing with x, the attempt frequency $\nu^0(x)$ and the entropic term $\exp[\Delta S(x)/k]$ giving $\sigma_0(x) \propto l(x)^2\nu^0(x)C(x)\exp\left(\frac{\Delta S(x)}{k}\right) \approx$ const [49].

Fig. 9(a) also shows that the ternary crystals, $NaAsSe_2$ ($x = 0.5$) and Na_3AsSe_3 ($x = 0.75$), are electronic insulators ($\sigma_{298} \approx 10^{-15}$ S cm^{-1}). The room-temperature conductivity σ_{298} of the $NaAsSe_2$ crystal (this work) is comparable to that reported in Ref. [50] after being recalculated to room temperature, Table 3. The room-temperature conductivity σ_{298} increases with sodium selenide content, $\sigma_{NaAsSe2} < \sigma_{Na3AsSe3} < \sigma_{Na2Se}$. However, compared to Na_2Se–As_2Se_3 alloys, σ_{298} values of the crystals are lower by approximately 2–3 orders of magnitude depending on the composition. Meanwhile, the activation energy for the crystals decreases from 1.3 eV ($x = 0.5$) to 0.75 eV ($x = 1.0$).

3.5. *Effect of crystallization on properties*

To investigate the impact of crystallization process on the structure and properties of the glass samples, we carried out thermal treatments on the $x = 0.2$ glassy composition at 275 °C using a conventional oven. Fig. 10 shows that the 5-h heating duration lead to the appearance of multiple Bragg peaks that were primarily associated with the orthorhombic $NaAsSe_2$, space group *Pbca*, and the $AsSe_{2.5}$ crystal structure [51]. However, the situation became more intricate following the 15-h treatment, with the persistence of the $AsSe_{2.5}$ crystalline phase, the disappearance of the previously precipitated $NaAsSe_2$ phase, and majority of reflections remained unidentified.

Fig. 11 effectively illustrates the impact of thermal treatment on the characteristics of precipitated particles of the $x = 0.2$ composition. The SEM image, corresponding to 5-h heating process, exhibits a consistent surface texture with the particles being well-defined and evenly distributed throughout the image. In contrast, after 15 h, the particles seem to lack a clear pattern or organization. They exhibit irregular shapes, varying sizes, and a more heterogeneous surface texture.

The observed structural characteristics significantly influence the electrical properties. Compared to the glassy sample, the heating process of 5 h adversely affected the room-temperature conductivity σ_{298} which decreased by approximately 2 orders of magnitude from 1.14×10^{-11} S cm^{-1} to 1.7×10^{-13} S cm^{-1}. In contrast, the 15-h treatment process resulted in a seven-fold conductivity increase, Fig. 11.

To facilitate the growth of the $NaAsSe_2$ crystal phase within amorphous alloys, the $x = 0.2$ and $x = 0.3$ glassy compositions underwent annealing treatments using Zirconium-Microwave MESTRA oven. The heating durations were 30 min, 1.5 h and 2 h, respectively. Fig. 12(a) and **12(b)** show the XRD patterns of the various annealed samples. Only the $x = 0.3$ sample, annealed for 2 h, exhibited distinct and well-defined Bragg peaks that are characteristic of crystalline $NaAsSe_2$ suggesting a composition dependence of crystal growth. SEM studies unveiled, for the $x = 0.3$ composition annealed for 2 h, the presence of wall-like structures, Fig. 13(b). Additionally, wave-like features containing nanometric droplets were observed, and the micrograph at a magnification of × 12000 provides visual evidence of this observation, Fig. 13(c).

One also observes, from Fig. 13(a), that the room-temperature conductivity of this annealed sample, $\sigma_{298} = 6.14 \times 10^{-12}$ S cm^{-1}, is ~ 3 orders of magnitude higher than that of the crystalline c-$NaAsSe_2$, and is only lower by 2 factors compared to the original $x = 0.3$ glassy composition, Table 3. The enhanced conductivity observed in glasses, as opposed to crystals, can potentially be explained by the presence of

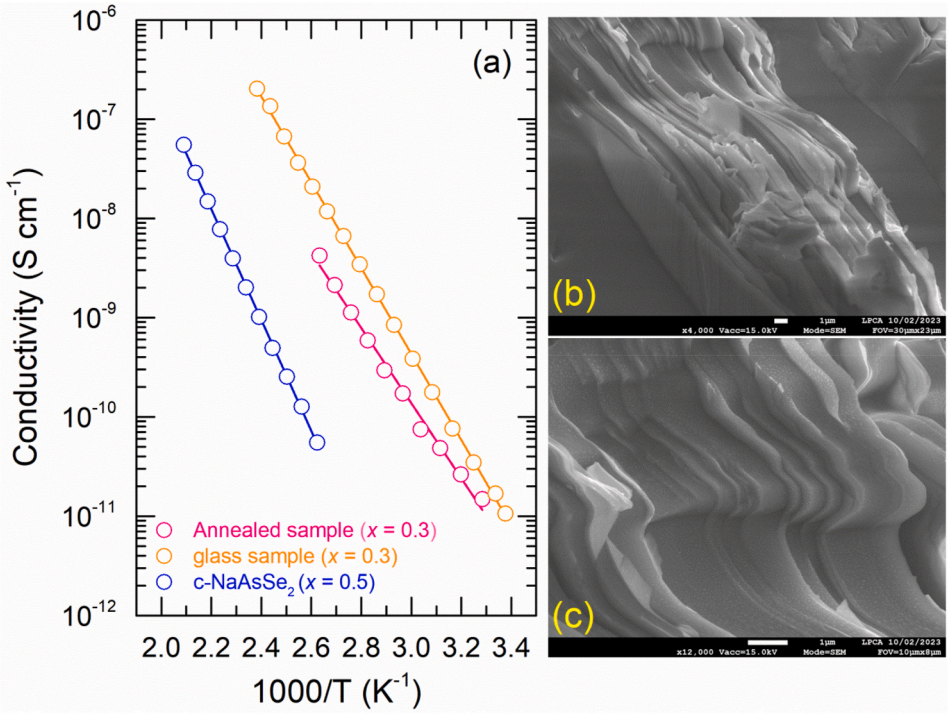

Fig. 13. (a) Conductivity results for the $x = 0.3$ composition annealed for 2 h (magenta colour) along with the original glassy composition (orange colour) and the crystalline $NaAsSe_2$ compound (blue colour). Scanning electron microscope (SEM) micrographs for the annealed sample (b) magnification of × 4000 and (c) magnification of × 12000. (For interpretation of the references to colour in this figure legend, the reader is referred to the Web version of this article.)

sodium ions dissociated by non-bridging selenide atoms. Evidence to those latter is provided by glass-transition decrease. It is widely recognized that when metal oxides or metal chalcogenides, such as Na_2Se, are introduced into an oxide or chalcogenide network, the interconnected network structure is disrupted, leading to the conversion of some bridging oxygen or chalcogen atoms into non-bridging species. The modest decrease in conductivity, by 2 factors, during the process of crystallization implies a slight reduction in the number of free sodium ions when the glass structure undergoes rearrangement to facilitate the growth of the $NaAsSe_2$ crystal. Similar behaviour was observed upon the crystallization of lithium metasilicate glasses, but the decrease in ionic conductivity was considerably more notable [52].

4. Conclusions

Bulk glasses were successfully obtained in the $(Na_2Se)_x(As_2Se_3)_{1-x}$ system, where $0 \leq x \leq 0.3$, using the melt-quenching technique. For the $x = 0.4$ composition, $NaAsSe_2$ crystallite phase was present. However, this phase mostly disappeared when the mechanical milling technique was utilized. With continuous Na_2Se additions, the density decreases, while the molar volume contracts, resulting in a denser glass material compared to cubic sodium selenide and other ternary Na–As–Se crystals as evidenced from the glass packing density. The glass compositions present single glass transition T_g demonstrating their homogeneity character despite the contradictory evidence revealed by SEM at $x \geq 0.2$. The electrical conductivity of Na_2Se–As_2Se_3 alloys exhibits an overall increase by two orders of magnitude as x content varies. However, the relationship between conductivity and composition is complicated. In NaSe-poor glasses, there is a consistent rise in conductivity at room temperature. Meanwhile, for glass compositions with $x \geq 0.2$, the conductivity parameters remain nearly unchanged, which might be attributed to the glass inhomogeneity as revealed by SEM analysis. The room-temperature conductivities of ternary Na–As–Se crystals are influenced by the Na_2Se content and are 2–3 orders of magnitude lower when compared to Na_2Se–As_2Se_3 alloys. The effects of different thermal treatment conditions on the properties of these alloys are also examined. Upon annealing, the glassy composition with $x = 0.3$ undergoes the formation of $NaAsSe_2$ crystalline phase, and its σ_{298} is similar to that of the original glass, but three orders of magnitude higher than the original crystalline c-$NaAsSe_2$.

Funding information

The Ph.D. work of Ali Sammoury (First co-author) is co-funded by the Université du Littoral Côte d'Opale (ULCO) and the Lebanese University.

Declaration of competing interest

The authors declare that they have no known competing financial interests or personal relationships that could have appeared to influence the work reported in this paper.

Acknowledgments

This work was supported by the Région Hauts de France and the Ministére de l'Enseignement Supérieur et de la Recherche (CPER Manifest) as well as by the A2U University Alliance (Artois-ULCO-UPJV).

Appendix A. Supplementary data

Supplementary data to this article can be found online at https://doi.org/10.1016/j.oceram.2023.100434.

References

[1] Q.-T. Xu, S.-S. Han, J.-N. Li, S.-P. Guo, $NaGa_3Se_5$: an infrared nonlinear optical material with balanced performance contributed by complex $\{[Ga_3Se_5]^-\}_\infty$ anionic network, Inorg. Chem. 61 (2022) 5479–5483, https://doi.org/10.1021/acs.inorgchem.2c00623.

[2] S.F. Li, X.M. Jiang, B.W. Liu, D. Yan, C.S. Lin, H.Y. Zeng, G.C. Guo, Superpolyhedron-built second harmonic generation materials exhibit large mid-

infrared conversion efficiencies and high laser-induced damage thresholds, Chem. Mater. 29 (2017) 1796–1804, https://doi.org/10.1021/acs.chemmater.6b05405.
[3] N. Takahashi, H. Ito, A. Miura, N.C. Rosero-Navarro, Y. Goto, Y. Mizuguchi, C. Miroyoshi, Y. Kuroiwa, M. Nagao, S. Watauchi, I. Tanaka, K. Tadaga, Synthesis, crystal structure and optical absorption of $NaInS_{2-x}Se_x$, J. Alloys Compd. 750 (2018) 409–413, https://doi.org/10.1016/j.jallcom.2018.03.407.
[4] B.A. Rosales, M.A. White, J. Vela, Solution-grown sodium bismuth dichalcogenides: toward earth-abundant, biocompatible semiconductors, J. Am. Chem. Soc. 140 (2018) 3736–3742, https://doi.org/10.1021/jacs.7b12873.
[5] T. Zhong, M. Pan, G. Gao, H. Fu, M. Wu, J.-M. Liu, Sodium bismuth dichalcogenides: candidates for ferroelectric high-mobility semiconductors for multifunctional applications, Phys. Chem. Chem. Phys. 21 (2019) 8553–8558, https://doi.org/10.1039/C9CP00336C.
[6] W.W.W. Leung, C.N. Savory, R.G. Palgrave, D.O. Scanlon, An experimental and theoretical study into $NaSbS_2$ as an emerging solar absorber, J. Mater. Chem. C 7 (2019) 2059, https://doi.org/10.1039/C8TC06284F.
[7] J. Sun, D.J. Singh, Electronic properties, screening, and efficient carrier transport in $NaSbS_2$, Phys. Rev. Appl. 7 (2017), 024015, https://doi.org/10.1103/PhysRevApplied.7.024015.
[8] C.-M. Dai, P. Xu, M. Huang, Z.-H. Cai, D. Han, Y. Wu, S. Chen, $NaSbSe_2$ as a promising light-absorber semiconductor in solar cells: first-principles insights, Apl. Mater. 7 (2019), 081122, https://doi.org/10.1063/1.5119383.
[9] A. Putatunda, G. Xing, J. Sun, Y. Li, D.J. Singh, Thermoelectric properties of layered $NaSbSe_2$, J. Phys. Condens. Matter 30 (2018), 225501, https://doi.org/10.1088/1361-648X/aabf5b.
[10] I.S. Khare, N.J. Szymanski, D. Gall, R.E. Irving, Electronic, optical, and thermoelectric properties of sodium pnictogen chalcogenides: a first principles study, Comput. Mater. Sci. 183 (2020), 109818, https://doi.org/10.1016/j.commatsci.2020.109818.
[11] T.K. Bera, J.I. Jang, J.-H. Song, C.D. Malliakas, A.J. Freeman, J.B. Ketterson, M. G. Kanatzidis, Soluble semiconductors $AASe_2$ (A = Li, Na) with a direct-band-gap and strong second harmonic generation: a combined experimental and theoretical study, J. Am. Chem. Soc. 132 (2010) 3484–3495, https://doi.org/10.1021/ja9094846.
[12] T. Famprikis, P. Canepa, J.A. Dawson, M.S. Islam, C. Masquelier, Fundamentals of inorganic solid-state electrolytes for batteries, Nat. Mater. 18 (2019) 1278–1291, https://doi.org/10.1038/s41563-019-0431-3.
[13] J.B. Goodenough, Rechargeable batteries: challenges old and new, J. Solid State Electrochem. 16 (2012) 2019–2029, https://doi.org/10.1007/s10008-012-1751-2.
[14] M.M. Doeff, R.J. Clément, P. Canepa, Solid electrolytes in the spotlight, Chem. Mater. 34 (2022) 463–467, https://doi.org/10.1021/acs.chemmater.1c03770.
[15] S. Zhang, Y. Yao, Y. Yu, Frontiers for room-temperature Sodium−Sulfur batteries, ACS Energy Lett. 6 (2021) 529–536, https://doi.org/10.1021/acsenergylett.0c02488.
[16] A. Banerjee, K.H. Park, J.W. Heo, Y.J. Nam, C.K. Moon, S.M. Oh, S.-T. Hong, Y. S. Jung, Na_3SbS_4: a solution processable sodium superionic conductor for all-solid-state sodium-ion batteries, Angew. Chem., Int. Ed. 55 (2016), https://doi.org/10.1002/anie.201604158, 9634−9638.
[17] X. Chi, Y. Liang, F. Hao, Y. Zhang, J. Whiteley, H. Dong, P. Hu, S. Lee, Y. Yao, Tailored organic electrode material compatible with sulfide electrolyte for stable all-solid-state sodium batteries, Angew. Chem., Int. Ed. 57 (2018) 2630–2634, https://doi.org/10.1002/anie.201712895.
[18] Hayashi, K. Noi, A. Sakuda, M. Tatsumisago, Superionic glass-ceramic electrolytes for room-temperature rechargeable sodium batteries, Nat. Commun. 3 (2012) 856–861, https://doi.org/10.1038/ncomms1843.
[19] L. Zhang, K. Yang, J. Mi, L. Lu, L. Zhao, L. Wang, Y. Li, H. Zeng, Na3PSe4: a novel chalcogenide solid electrolyte with high ionic conductivity, Adv. Energy Mater. 5 (2015) 2–6, https://doi.org/10.1002/aenm.201501294.
[20] W.D. Richards, T. Tsujimura, L.J. Miara, Y. Wang, J.C. Kim, S.P. Ong, I. Uechi, N. Suzuki, G. Ceder, Design and synthesis of the superionic conductor $Na_{10}SnP_2S_{12}$, Nat. Commun. 7 (2016), 11009, https://doi.org/10.1038/ncomms11009.
[21] T.W. Kim, K.H. Park, Y.E. Choi, J.Y. Lee, Y.S. Jung, Aqueous-solution synthesis of Na_3SbS_4 solid electrolytes for all-solid-state Na-ion batteries, J. Mater. Chem. A 6 (2018) 840–844, https://doi.org/10.1039/C7TA09242C.
[22] E.P. Ramos, Z. Zhang, A. Assoud, K. Kaup, F. Lalére, L.F. Nazar, Correlating ion mobility and single crystal structure in sodium-ion chalcogenide-based solid state fast ion conductors: $Na_{11}Sn_2PnS_{12}$ (pn = Sb, P), Chem. Mater. 30 (2018) 7413–7417, https://doi.org/10.1021/acs.chemmater.8b02077.
[23] E.P. Ramos, A. Assoud, L. Zhou, A. Shyamsunder, D. Rettenwander, L.F. Nazar, Structure–transport correlations in $Na_{11}Sn_2SbSe_{12}$ and its sulfide solid solutions, Apl. Mater. 11 (2023), 011104, https://doi.org/10.1063/5.0129001.
[24] M. Duchardt, U. Ruschewitz, S. Adams, S. Dehnen, B. Roling, Vacancy-controlled Na^+ superionic conduction in $Na_{11}Sn_2PS_{12}$, Angew. Chem. Int. Ed. 57 (2018) 1351–1355, https://doi.org/10.1002/anie.201712769.
[25] S.K. Kim, A. Mao, S. Sen, S. Kim, Fast Na-ion conduction in a chalcogenide glass-ceramic in the ternary system Na_2Se-Ga_2Se_3-$GeSe_2$, Chem. Mater. 26 (2014) 5695–5699, https://doi.org/10.1021/cm502542p.
[26] I.A. Sokolov, I.V. Murin, YuK. Startsev, M.Yu Zubkova, A.A. pronkin, Glass Formation and electrical conductivity of glasses in the Na_2Se–P_2Se_5 system in a wide temperature range, Glass Phys. Chem. 36 (2010) 21–26, https://doi.org/10.1134/S1087659610010049.
[27] Y. Hibi, N. Tanibata, A. Hayashi, M. Tatsumisago, Preparation of sodium ion conducting Na_3PS_4-NaI glasses by a mechanochemical technique, Solid State Ionics 270 (2015) 6–9, https://doi.org/10.1016/j.ssi.2014.11.024.
[28] M. Kassem, T. Bounazef, A. Sokolov, M. Bokova, D. Fontanari, A.C. Hanon, I. Alekseev, E. Bychkov, Deciphering fast ion transport in glasses: a case study of sodium and silver vitreous sulfides, Inorg. Chem. 61 (2022) 12870–12885, https://doi.org/10.1021/acs.inorgchem.2c02142.
[29] M. Kassem, T. Bounazef, D. Fontanari, A. Sokolov, M. Bokova, A.C. Hanon, E. Bychkov, Chemical and structural variety in sodium thioarsenate glasses studied by neutron diffraction and supported by first-principles simulations, Inorg. Chem. 59 (2020) 16410–16420, https://doi.org/10.1021/acs.inorgchem.0c02220.
[30] Z.U. Borisova, Glassy Semiconductors, Plenum Press, New York, 1981.
[31] V. Mastelaro, S. Bénazeth, H. Dexpert, EXAFS study of Ag-As-Se and Ag-As-S ionic conductor glasses, J. Phys. IV France 2 (1992) C2–C195, https://doi.org/10.1051/jp4:1992228. -C2-200.
[32] Z. Liu, W. Hu, H. Deng, Chemistry of defects in crystalline Na_2Se: implications for the Na−Se battery, J. Phys. Chem. C 124 (2020) 27930–27936, https://doi.org/10.1021/acs.jpcc.0c09021.
[33] The Materials Project, Materials Data on Na2Se by Materials Project, 2020, https://doi.org/10.17188/1189110. United States: N. p.
[34] L. Calvert, National Research Council of Canada, ICDD Grant-in-Aid, Ottawa, Canada, 1980.
[35] Editor Lide DR. CRC Handbook of Chemistry and Physics 78th edn. New York: CRC Press, 1997–1998.
[36] The Materials Project, Materials Data on $NaAsSe_2$ by Materials Project, 2020, https://doi.org/10.17188/1201589. United States: N. p.
[37] The Materials Project, Materials Data on Na_3AsSe_3 by Materials Project, 2020, https://doi.org/10.17188/1312502. United States: N. p.
[38] The Materials Project, Materials Data on Na2Se by Materials Project, 2020, https://doi.org/10.17188/1189110. United States: N. p.
[39] M. Kassem, Nouveaux Verres Chalcogénures CdX-AgI-As2X3 (X = Se Ou Te) : Transport - Structure - Sensibilité Ionique, PhD Thesis (theses.fr/151480419), University of Littoral, 2010.
[40] M.A.T. Marple, D.C. Kaseman, I. Hung, Z. Gan, S. Sen, Structure and physical properties of glasses in the system Ag_2Se–Ga_2Se_3–$GeSe_2$, J. Non-Cryst. Solids 437 (2016) 34–42, https://doi.org/10.1016/j.jnoncrysol.2016.01.006.
[41] M.A.T. Marple, D.C. Kaseman, I. Hung, Z. Gan, S. Sen, Synthesis and characterization of ternary glasses in the system Na_2Se-Ga_2Se_3-$GeSe_2$, J. Non-Cryst. Solids 404 (2014) 91–97, https://doi.org/10.1016/j.jnoncrysol.2014.07.042.
[42] I.A. Sokolova, I.V. Murinb, YuK. Startsevc, M.Yu Zubkovac, A.A. Pronkinc, Glass Formation and electrical conductivity of glasses in the Na_2Se–P_2Se_5 system in a wide temperature range, Glass Phys. Chem. 36 (2010) 21–26, https://doi.org/10.1134/S1087659610010049.
[43] E. Bychkov, D.L. price, A. Lapp, Universal trend of the Haven ratio in glasses: origin and structural evidences from neutron diffraction and small-angle neutron scattering, Journal of Non-Crystalline Solids 293-295 (2001) 211–219, https://doi.org/10.1016/S0022-3093(01)00673-1.
[44] E. Bychkov, A. Bychkov, A. Pradel, M. Ribes, Percolation transition in Ag-doped chalcogenide glasses: comparison of classical percolation and dynamic structure models, Solid State Ionics 113–115 (1998) 691–695, https://doi.org/10.1016/S0167-2738(98)00396-8.
[45] A. Piarristeguy, M. Ramonda, N. Kuwata, A. Pradel, M. Ribes, Microstructure of Ag_2S–As_2S_3 glasses, Solid State Ionics 177 (2006) 3157–3160, https://doi.org/10.1016/j.ssi.2006.07.054.
[46] A. Paraskiva, M. Bokova, E. Bychkov, Na^+ ion conducting glasses in the NaCl-Ga_2S_3-GeS_2 system: a critical percolation regime, Solid State Ionics 299 (2017) 2–7, https://doi.org/10.1016/j.ssi.2016.11.003.
[47] B. Barrau, M. Ribes, M. Maurin, A. Kone, J.L. Souquet, Glass formation, structure and ionic conduction in the Na_2S-GeS_2 system, J. Non-Cryst. Solids 37 (1980) 1–14, https://doi.org/10.1016/0022-3093(80)90473-1.
[48] H.K. Patel, S.W. Martin, Fast ionic conduction in Na_2S+B_2S_3 glasses: compositional contributions to non-exponentiality in conductivity relaxation in the extreme low-alkali-metal limit, Phys. Rev. B 44 (1992) 10292–10300, https://doi.org/10.1103/PhysRevB.45.10292.
[49] C. Déportes, M. Duclot, P. Fabry, J. Fouletier, A. Hammou, M. Kleitz, E. Siebert, J. L. Souquet, Grenoble EDP Sciences, Électrochimie des solides, 1994.
[50] C. Pompe, Strukturchemie und elektrische Leitfähigkeiten von Natriumchalkogenometallaten, PHD thesis, 2018 (Université de Ratisbonne).
[51] M.F. Kotkata, A.M. Shamah, M.B. El-Den, M.K. El-Mously, An X-ray study of As-Se-Te compounds, Acta Phys. Hung. 54 (1983) 49–63, https://doi.org/10.1007/BF03158692.
[52] P. Pernice, A. Aronne, A. Marotta, Electrical conductivity change with crystallization in lithium metasilicate glass, Solid State Ionics 37 (1989) 79–81, https://doi.org/10.1016/0167-2738(89)90291-9.